ELSEVIER

Journal of Physics and Chemistry of Solids 60 (1999) 861–866

JOURNAL OF PHYSICS AND CHEMISTRY OF SOLIDS

Vibrational spectra of superionic crystals $(BaF_2)_{1-x}$ $(LaF_3)_x$

F. Kadlec[a,b,*], P. Simon[a], N. Raimboux[a]

[a]*CNRS-CRMHT, 45071 Orléans Cedex 2, France*
[b]*Institute of Physics, Academy of Sciences of the Czech Republic, 182 21 Prague 8, Czech Republic*

Received 29 October 1998; accepted 1 February 1999

Abstract

Infrared reflectivity and Raman spectra of $(BaF_2)_{1-x}(LaF_3)_x$ $(0.01 \leq x \leq 0.47)$ single crystals are reported. Vibrational modes due to doping have been observed; a number of them can be interpreted as non-centre zone modes activated by loss of translational symmetry. Others are attributed to changes of local structure around clusters of dopant ions, which give rise to modes inherent to LaF_3. Evolution of infrared spectra with doping rate x is discussed in terms of a percolation model.

Keywords: A. Inorganic compounds; C. Raman spectroscopy; C. Infrared spectroscopy; D. Defects

1. Introduction

In recent years, rare-earth doped fluorine conductors with the fluorite structure have been attracting the interest of researchers as a model system with superionic conductivity and partial disorder. Their general formula is $(MF_2)_{1-x}(RF_3)_x$ where M = Ca, Sr, Ba, Pb and x is the rate of doping by the rare-earth element R. The overall cubic crystal symmetry (space group Fm3m) is conserved within $0 \leq x \leq x_{max}$, where $x_{max} \approx 0.4$–0.5 depending on M, R [1]. The room temperature conductivity, due to hopping of F^- anions, increases by several orders of magnitude with doping.

Around the trivalent R^{3+} cations, clusters of defects are formed. Their structure depends, in general, on M and R [2,3]. The lattice in the vicinity of the clusters is deformed, thus forming so-called defect regions [4] in the undeformed fluorite matrix. According to the Enhanced Ionic Motion model [5], these distortions are supposed to enhance the ionic conductivity by decreasing locally (at the interface between the clusters and matrix) the value of the activation enthalpy for hops of F^- anions.

The solid solutions $(BaF_2)_{1-x}(LaF_3)_x$ belong to the most studied systems of this family. Despite the long-range crystalline order, it has been found that features characteristic for glasses and amorphous solids develop with increasing x. On the basis of low temperature thermal conductivity, specific heat and internal friction measurements, the presence of low-energy excitations has been suggested earlier [6] corresponding to the model of two-level systems [7]. This model has been also used to explain the results of low temperature far-infrared absorption measurements [8].

The previous Raman scattering studies have shown that only the T_{2g} mode active in the Raman spectrum of BaF_2 becomes asymmetric on doping and gradually splits into two peaks [9–11]. On heating, near the superionic transition, the width of the peaks deviates from a linear behaviour [9,10]. In another work, it was suggested that the low-frequency region of the spectra displays a crossover near 60 cm^{-1} which can be interpreted in terms of the fracton model [11].

In the present article, we present the results of our study of infrared and Raman spectra of six $(BaF_2)_{1-x}(LaF_3)_x$ single crystals with $0.01 \leq x \leq 0.47$. To our knowledge, complete infrared spectra of compounds of this family are reported for the first time here.

2. Experimental

The single crystalline samples were grown from melts by the Bridgman technique [12] under fluorinating atmosphere in the Institute of Crystallography, Moscow. Using this technique, the solid solutions contain about 0.01–0.02 wt.% of

* Corresponding author. Tel.: + 420-2-6605-2144; fax: + 420-2-821-227.

E-mail address: kadlecf@fzu.cz (F. Kadlec)

0022-3697/99/$ - see front matter
PII: S0022-3697(99)00020-7

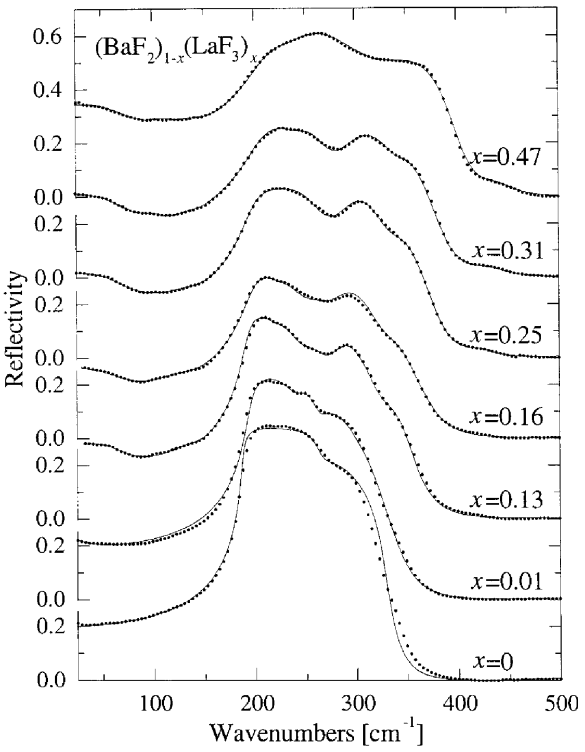

Fig. 1. Infrared reflectivity spectra of $(BaF_2)_{1-x}(LaF_3)_x$ single crystals.

residual oxygen [12]. The crystals had a form of parallelepiped with a size of about $6 \times 6 \times 4$ mm^3. Their composition was verified by means of electron microscope. The doping rate was established with an accuracy better than $\pm$ 0.5%.

Near-normal incidence infrared reflectivity spectra were measured at a resolution of 6 cm^{-1} using the Fourier-transform spectrometer Bruker IFS-113v. The measurements were carried out under low vacuum in a spectral range of 30–3000 cm^{-1}. A liquid He cooled Si bolometer was used as a detector in the spectral region 30–600 cm^{-1}.

Raman spectra in parallel (VV) and crossed (VH) polarization setup were measured in the 90° scattering geometry using a Jobin–Yvon T 64000 Raman spectrometer operating in the triple subtractive mode and equipped by a liquid nitrogen cooled CCD detector. For excitation, the 514.5 and 568.2 nm lines of an Ar–Kr laser were used, with the beam power incident on the sample of about 100 and 40 mW, respectively. Attempts were made to use several excitation frequencies of the laser, but in all Stokes spectra, the Raman signal was mixed with broad luminescence peaks induced by rare earth impurities. For the above two excitation frequencies, it appeared possible to measure anti-Stokes Raman spectra free of parasite signal; they were recorded in the Raman shift range 15–600 cm^{-1}.

3. Results and evaluation

Infrared reflectivity spectra are shown in Fig. 1. The symbols represent experimental data and solid lines show calculated spectra obtained by means of fitting. To this purpose, we have used the factorized form of the (complex) dielectric function [13]

$$\varepsilon(\omega) = \varepsilon_\infty \prod_{j=1}^{J} \frac{\omega_{j\mathrm{LO}}^2 - \omega^2 + i\omega\Gamma_{j\mathrm{LO}}}{\omega_{j\mathrm{TO}}^2 - \omega^2 + i\omega\Gamma_{j\mathrm{TO}}} \quad (1)$$

with the number of modes J reaching up to 7 (for $x = 0.47$). In Eq. (1), $\omega_{j\mathrm{LO}}$ and $\omega_{j\mathrm{TO}}$ are the transverse and longitudinal optical frequencies, $\Gamma_{j\mathrm{LO}}$ and $\Gamma_{j\mathrm{TO}}$ denote longitudinal and transverse damping constants, respectively; and ϵ_∞ is the permittivity limit at high frequency.

The experimentally obtained Raman spectra for the two polarizations, reduced by the Bose–Einstein factor and by the frequency dependent scattering factor, are shown in Fig. 2. These spectra were obtained using the 514.5-nm laser frequency and almost identical results were obtained using the 568.2-nm line. In order to determine the positions of the peaks, the spectra were fitted using the sum of Lorentzian curves. These positions are shown by triangles in Fig. 2. For comparison, all mode frequencies obtained by evaluation of both Raman and infrared spectra are shown in Fig. 3.

4. Discussion

4.1. Infrared spectra

In pure BaF_2, only one infrared active mode is allowed by the crystal symmetry, but we see that the main reflectivity band of BaF_2 exhibits a small feature near 260 cm^{-1} as a result of a two-phonon combination. This feature has been observed in all stoichiometric fluorite-structured crystals [15].

At doping rate $x = 0.01$, distinct differences from the spectrum of pure BaF_2 appear. Two new peaks are present, one in the main reflectivity band near 240 cm^{-1}, and another at low frequencies ($\omega_{\mathrm{TO}} \approx 27$ $^{-1}$, $\omega_{\mathrm{TO}} \approx 30$ $^{-1}$). The former is similar to that observed at 260 cm^{-1}, and we suggest that it originates in a perturbation of the symmetry-allowed mode. The latter is not easily seen in the spectrum by naked eye due to relatively high damping, but fitting reveals that a change in the slope of $R(\omega)$ is clearly present below ca. 80 cm^{-1}. As at this doping level the clusters occupy only a small volume fraction of the sample, we attribute this peak to a localized vibrational mode induced by clusters. It is probably connected with small displacements of the clusters as a whole, for example with their librations or translations. The low frequency of these vibrations supports this idea, because only objects with a mass substantially higher than atoms can exert vibrations with such a low frequency. We would like to note that a mode with similar frequency lower

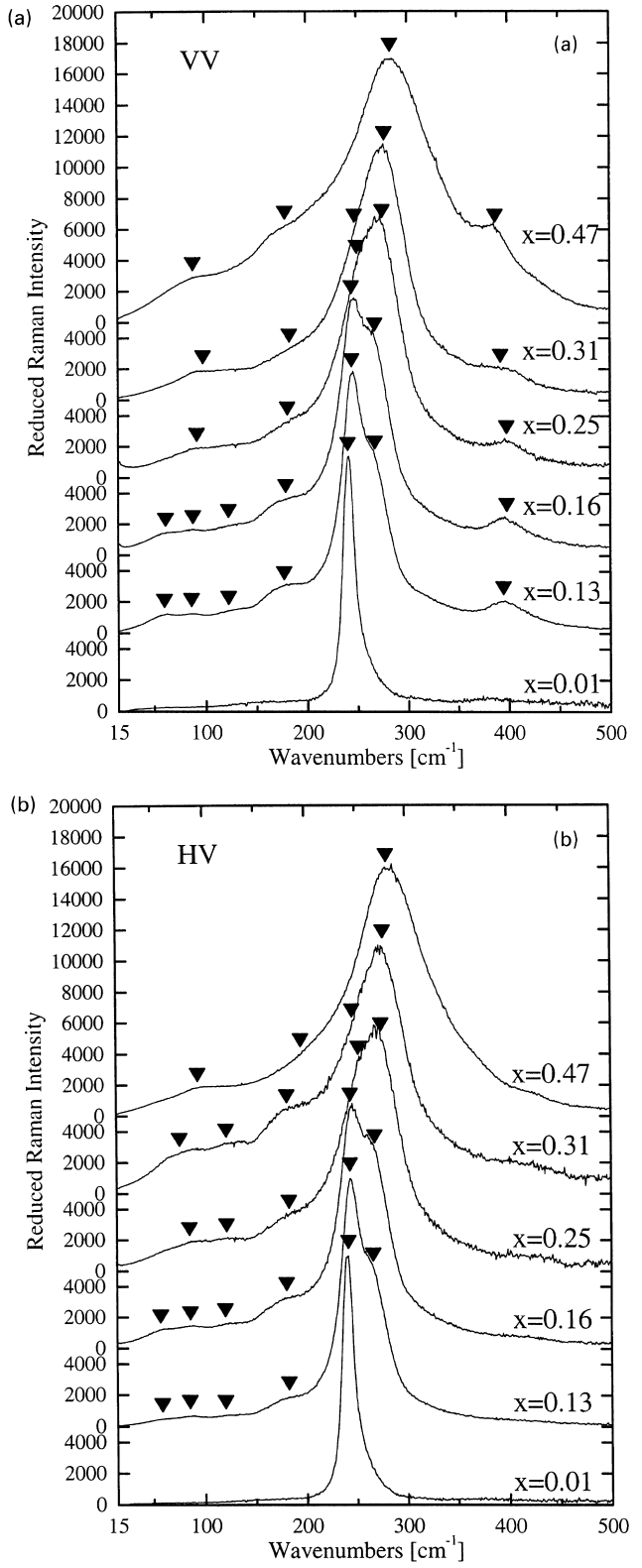

Fig. 2. Bose–Einstein reduced anti-Stokes-shift Raman spectra of $(BaF_2)_{1-x}(LaF_3)_x$ single crystals: (a) VV polarization, (b) HV polarization. The triangles mark positions of peaks obtained by fits.

than that of the transverse acoustic mode, has been observed in the $x = 0.16$ sample by inelastic neutron scattering [16].

With further doping, the broad lowest-frequency mode becomes more distinct and shifts to higher frequencies ($\approx$ 70–80 cm^{-1}). Below ca. 30 cm^{-1}, a weak departure of the experimental data from the fit towards higher intensity can be seen. It is questionable whether this is a sign of further presence of the localized vibrational mode, as this spectral region is close to the limit of the operating range of the detector. Other broad peaks located below the main reflectivity band appear at $x = 0.13$ near 130 cm^{-1}, at $x = 0.31$ near 110 cm^{-1}, and a few other peaks develop on doping in the spectral region 200–300 cm^{-1}, corresponding to the main band. The frequencies of all these peaks between 65 and 270 cm^{-1} correspond very well to those energies where the phonon dispersion curves of BaF_2 are flat, with the wavevector different from zero [17]. This shows clearly that all these modes become infrared active due to loosening of selection rules following the loss of translation symmetry.

We see that with increasing x, all modes tend to harden. This effect can be seen most clearly on ω_{LO} of the main band, which shifts from 330 cm^{-1} at $x = 0$ up to 402 cm^{-1} at $x = 0.47$. We suppose that this is due to the decrease of the lattice parameter a with increasing x (a (Å) = $6.20 - 0.31x$, [1]).

4.2. Percolation effects

We would like to turn our special attention to the mode which develops on the high-frequency side of the main infrared reflectivity band, near 420 cm^{-1}, starting from $x = 0.25$ (see Fig. 1). In the spectrum of the $x = 0.16$ sample, this mode is absent, therefore, there must be some changes in the local defect configuration occurring between these two values. We presume that the explanation can be found using the percolation model with two critical points [18]. This model treats ion-conducting solids consisting of a mixture of normally conducting matrix containing a volume concentration, p, of a randomly dispersed insulating material, with a highly conducting interface in between. The main conclusion of this model is the existence of two critical concentrations (percolation thresholds) p'_c, p''_c, related by $p''_c = 1 - p'_c$. At p'_c percolation of the highly conductive interfaces occurs. This manifests itself in a sudden increase in the conductivity $\sigma(p)$. Starting from the second critical concentration, p''_c, the volume occupied by the insulating material is so large that the conducting paths are disrupted, which, by contrast, leads to a decrease in $\sigma(p)$.

This model can be applied to the $(BaF_2)_{1-x}(LaF_3)_x$ systems if one considers that the BaF_2 matrix is low conducting. The clusters of defects are stable, at least at room temperature, i.e. they do not permit ion transport and behave like insulating domains. The interfaces between cluster and the matrix are highly conducting, according to the Enhanced Ionic Motion model [5] which we believe to be valid. In order to apply the percolation model [18] we have to consider the volume concentration p of clusters, which is clearly proportional to x; one can write $p = \alpha x$ where α is a proportionality factor to be determined. From $\sigma(x)$ measurements, the percolation threshold has been established at $x'_c \approx 0.05$ [19]. The volume fraction corresponding to this percolation can be estimated as $0.2 \leq p'_c \leq 0.25$ [20], so the value of α is between 4 and 5. Then, the value of $p''_c \equiv 1 - p'_c$ lies between 0.8 and 0.75, which corresponds to $0.15 \leq x''_c \leq 0.20$.

In consequence, based on the percolation model [18], we can expect that for $x > 0.2$, the volume occupied by clusters is no more discontinuous, which implies a qualitative change in the force constants. In our opinion, the infrared active mode near 420 cm^{-1} is because of these changes. We

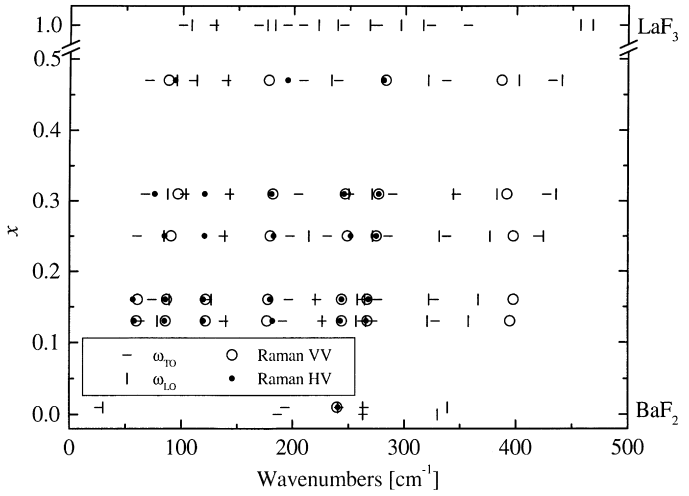

Fig. 3. Comparison of mode frequencies obtained from fits of room temperature vibrational spectra of $(BaF_2)_{1-x}(LaF_3)_x$. The values of ω_{TO}, ω_{LO} for $x = 1$ are taken from [14].

think further that there is a resemblance between this mode and the two highest-frequency modes of LaF_3. Indeed, in Fig. 3 we see that with increasing x, the longitudinal frequency ω_{LO} of this mode approaches those of LaF_3 [14]. This is in agreement with the former assumption that fragments of the tysonite (LaF_3) structure form in the fluorite-type $(MF_2)_{1-x}(RF_3)_x$ solid solutions [21]. We would like to note that we have also found an analogous behaviour in the reflectivity spectra of the $(BaF_2)_{1-x}(NdF_3)_x$ system.

Finally, let us comment on the limits of validity of the percolation model [18]. The model predicts that above p''_c, $\sigma(p)$ decreases. For $(BaF_2)_{1-x}(LaF_3)_x$, however, this has not been observed—$\sigma(x)$ rises slowly up to x_{max} [19,22]. If we assume that clusters form fragments of the tysonite structure (that of LaF_3), this is easy to explain, as it is known that even at room temperature, LaF_3 is a good ionic conductor ($\sigma \approx 10^{-6}$ (Ω cm^{-1}) [23]). This implies that if the clusters are sufficiently close, the network they form becomes partly conducting. That is why the experimental results disagree with the prediction of the percolation model [18] about conductivity decrease. Further, if p reaches the value of 1, it is not possible to define insulating domains, conductive domains and their interfaces in terms of the model [18]. Based on the estimate $4 \leq \alpha \leq 5$, this is the case starting from the dopant concentration $x = 1/\alpha$ lying between 0.2 and 0.25.

4.3. Raman spectra

As one can see from Fig. 2, the Raman spectra of the $x = 0.01$ sample are virtually the same for both configurations (VV, VH). The T_{2g} peak is located at the same frequency as in pure BaF_2, 240 cm^{-1}, but the weak doping makes it asymmetric. This result is in agreement with previous experimental work [9–11] where unpolarized spectra were measured. Aside this peak, the spectra display no distinct differences from that of BaF_2.

For doping rates $x = 0.13$ and higher, the spectra in the 200–300 cm^{-1} spectral region are very similar in both polarizations. Here, the shape of the spectra is close to those reported previously [9–11]; we see that a new peak appears near 260 cm^{-1}. With doping, its intensity increases, the peak shifts to higher frequencies and dominates the 240 cm^{-1} peak. The latter peak is absent in the spectra for $x = 0.47$; note that such a high doping rate has been examined for the first time. In the previous work Raman spectra were studied only up to $x = 0.359$ [10], where this component is still clearly present.

Outside the 200–300 cm^{-1} spectral domain, our results are rather different from those reported earlier by Kolesík et al. [11]. We attribute these differences to the fact that in Ref. [11], Stokes spectra are reported, which we have found to be mixed with luminescence signal. In contrast, in the present work we have measured anti-Stokes spectra and the spectra taken with green and yellow excitation lines were verified to be comparable.

Below 200 cm^{-1}, four broad peaks are present in the spectra for $x \geq 0.13$, with frequencies down to ca. 60 cm^{-1}. With increasing doping, the lowest-frequency peak in both polarizations disappears. The peak near 120 cm^{-1} is observable for $x \leq 0.16$ in the VV spectra and for $x \leq 0.31$ in the HV spectra. Given the closeness of their frequencies to those obtained from the infrared spectra (see Fig. 3), we attribute these peaks equally to modes off the Brillouin zone centre activated by the loss of translation symmetry.

The most important difference between both the polarizations consists in the peak in the VV spectra near 400 cm^{-1}, which is virtually absent in the HV spectra. It is clearly observable for all La concentrations from $x = 0.13 - 0.47$. With increasing x, its frequency decreases down to 387 cm^{-1}. In the Raman spectra of LaF_3, a very strong mode near just below 400 cm^{-1} has been observed in the $x(zz)y$ scattering geometry; in the $z(yx)y$ and $z(xz)y$ geometries it is substantially weaker and absent, respectively [24]. In accordance, we suppose that the observed peak could be caused by the local crystal structure within clusters similar to that of LaF_3. Note that the peak is present for $x \geq 0.13$; i.e., the concentration where it appears is lower than the one where, in the infrared spectra, the peak near 420 cm^{-1} appears, which we attribute also to developing tysonite structure. This is in agreement with the fact that, generally, Raman scattering is more sensitive to the short-range structure whereas infrared spectroscopy, as a result of Coulomb forces, is rather long-range sensitive.

5. Conclusion

By comparing the infrared and Raman spectra of samples in a wide range of dopant concentration, we have shown that the lowered crystal symmetry of the mixed crystals $(BaF_2)_{1-x}(LaF_3)_x$ manifests itself in their vibrational properties. In particular, the loss of translation symmetry activates modes which are not allowed by the $\vec{k} = 0$ selection rules. At the same time, the new modes with frequencies close to those observed in LaF_3 confirm the earlier predictions about existence of fragments with tysonite structure [21]. Considering the percolation effects, we have shown that the appearance of the infrared-active mode near 420 cm^{-1} at $x \approx 0.25$ is in agreement with the model of Enhanced Ionic Motion [5].

Acknowledgements

We are grateful to B.P. Sobolev from Institute of Crystallography, Moscow, for providing us with the samples and to K. Jurek from the Institute of Physics, Prague, for establishing the dopant concentrations.

References

[1] B.P. Sobolev, Butll. Soc. Cat. Cièn. 12 (3) (1991) 275–332.
[2] J.M. Réau, P. Hagenmuller, Appl. Phys. A 49 (1989) 3–12.
[3] P.P. Fedorov, Butll. Soc. Cat. Cièn. 12 (2) (1991) 349–381.
[4] A.K. Ivanov-Shits, N.I. Sorokin, P.P. Fedorov, B.P. Sobolev, Solid State Ionics 31 (1989) 253–268.
[5] K.E.D. Wapenaar, J. Schoonman, J. Electrochem. Soc. 126 (4) (1979) 667–672.
[6] D.G. Cahill, R.O. Pohl, Phys. Rev. B 39 (14) (1989) 10477–10480.
[7] W.A. Phillips, Rep. Prog. Phys. 50 (1987) 1657–1708.
[8] S.A. FitzGerald, J.A. Campbell, A.J. Sievers, Phys. Rev. Lett. 73 (23) (1994) 3105–3108.
[9] D. Marel, H.W. van den Hartog, Phys. Rev. B 25 (11) (1982) 6602–6608.
[10] D.J. Oostra, H.W. van Hartog, Phys. Rev. B 29 (5) (1984) 2423–2432.
[11] M. Kolesík, D. Tunega, B.P. Sobolev, Phys. Status Solidi (b) 160 (1990) 375.
[12] A.K. Ivanov-Shits, N.I. Sorokin, P.P. Fedorov, B.P. Sobolev, Fiz. Tv. Tela 25 (6) (1983) 1748–1753 in Russian.
[13] F. Gervais, Infrared and Millimeter Waves, 8, Academic, New York, 1983 pp. 279–339.
[14] R.P. Lowndes, J.F. Parrish, C.H. Perry, Phys. Rev. 182 (3) (1969) 913–922.
[15] W. Kaiser, W.G. Spitzer, R.H. Kaiser, L.E. Howarth, Phys. Rev. 127 (6) (1962) 1950–1954.
[16] F. Kadlec, F. Moussa, P. Simon, B.P. Sobolev, Solid State Ionics 119 (1–4) (1999) 131–137.
[17] J.P. Hurrell, V.J. Minkiewicz, Solid State Commun. 8 (1970) 463–466.
[18] H.E. Roman, A. Bunde, W. Dieterich, Phys. Rev. B 34 (5) (1986) 3439–3445.
[19] A.K. Ivanov-Shits, N.I. Sorokin, P.P. Fedorov, B.P. Sobolev, Solid State Ionics 31 (1989) 269–280.
[20] S. Kirkpatrick, Rev. Mod. Phys. 45 (4) (1973) 574–588.
[21] S.V. Chernov, W. Gunßer, I.V. Murin, Solid State Ionics 47 (1991) 67–70.
[22] K.E.D. Wapenaar, J.L. van Koesveld, J. Schoonman, Solid State Ionics 2 (1981) 145–154.
[23] C. Hoff, H.D. Wiemhoefer, O. Glumov, Solid State Ionics 101-103 (1997) 445–449.
[24] R.P. Bauman, S.P.S. Porto, Phys. Rev. 161 (3) (1967) 842–847.